10.6 Simulated squall lines with and without cloud shading effects

ANDREW J. OBERTHALER* AND PAUL M. MARKOWSKI

Department of Meteorology, The Pennsylvania State University, University Park, Pennsylvania

1. Introduction

Many popular radiative parameterizations, while accurate to a certain order, have inherent limitations when modeling the three dimensional effects of cloud shading. Monte Carlo methods (such as those described by Marchuk et al. 1980) are one such technique, in which 3d radiation can be calculated stochastically. However, this kind of statistical calculation is computationally expensive when run within a model instead of as a post–processing utility. A one–dimensional independent column approximation (ICA) is used in many global climate models in order to quickly produce domain–average radiation estimates (Marshak et al. 1995; Cahalan et al. 2005). However, ICA based models calculate radiation fluxes only in vertical columns, and do not allow for horizontal propagation of radiation between columns (Cahalan et al. 2005). The inability to calculate radiation based on varying solar zenith angles has been shown to be a significant source of error in local surface radiation estimates (O'Hirok and Gautier 2005; Frame et al. 2009).

The tilted independent pixel approximation (also known as the TIPA) proposed by Varnai and Davies (1999) attempts to resolve these issues by supporting slantwise propagation of radiation while allowing that same radiation field to influence model dynamics. The estimation appears to be a more appropriate estimation for assessing one–dimensional heterogeneity in cloud fields (Varnai and Davies 1999). The TIPA also produces distinct differences in local radiation fluxes (Frame et al. 2009) compared to a standard independent pixel approximation in which radiation only propagates vertically. The effect of anvil shading on convective storm environments is one current area of research which appropriately utilizes the TIPA to examine differences in storm evolution.

Observations have shown that near–surface temperature differentials can be as large as 3 K between clear air and anvil–shaded areas (Markowski et al. 1998; Bryan and Parker 2010). Markowski et al. (1998) conjectured that anvil shading could lead to significant baroclinic generation of horizontal vorticity. Markowski and Harrington (2005) made an initial attempt to include cloud shading effects in a supercell thunderstorm via a crude parameterization wherein the soil was artificially cooled at cloudy gridpoints. In recent years, several studies have examined the effects of anvil shading in convective environments using the TIPA (Frame et al. 2008; Frame and Markowski 2008; Frame et al. 2009; Frame and Markowski 2010). However, to the authors' knowledge, there has been no prior study focusing on anvil shading in squall line environments.

*Corresponding author address: Andrew Oberthaler, Department of Meteorology, Pennsylvania State University, 503 Walker Building, University Park, PA 16802; e-mail: ajo142@psu.edu.

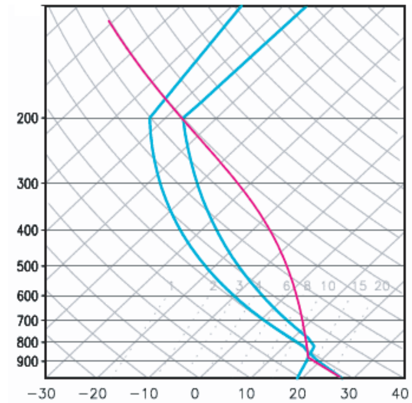

FIG. 1. Thermodynamic profile used at mdoel initialization time for each of the simulations.

The present study will attempt to further the growing knowledge of the effects of anvil shading in convective environments. The study will explore anvil shading effects ahead of a convective squall line using the TIPA to compute radiation. Squall lines will be initiated in different environmental wind shear regimes in order to examine the effects of anvil shading on the storm environment. It will be shown that the inclusion of cloud shading can lead to changes in the vertical wind profile ahead of the gust front, and, as a result, significant differences in squall line evolution and structure relative to squall lines simulated without cloud shading effects.

2. Model initialization

All model simulations were run with the Advanced Regional Prediction System (ARPS), version 5.1.5 (Xue et al. 2000, 2001). Each simulation domain had a uniform grid spacing of 1 km in each horizontal direction and a vertically stretched grid with a minimum grid spacing of 10 m at the lowest scalar grid point 5 m above the ground. Each domain employed periodic lateral boundary conditions along the north and south boundaries with open lateral boundary conditions along the east and west boundaries. The base state is horizontally homogeneous. Convection is initiated by introducing a line thermal (aligned in the y-direction) having a maximum potential temperature excess of 4 K, upon which additional random 0.1 K potential temperature perturbations are added (the random perturbations provide the heterogeneity needed for convection initiation). The simulations were initialized on 20 May at 1200 LST. All of the simulations were initialized using an identical thermodynamic profile (Fig. 1).

A 1.5–order turbulence closure was used, with eddy viscosities determined by the prognosed turbulent kinetic energy and a mixing length scale, with the latter depending on the boundary layer depth according to the method of Sun and Chang (1986). The microphysics parameterization includes ice and uses the Lin et al. (1983) scheme. Surface fluxes were computed using bulk aerodynamic formulae, with stability dependent surface drag coefficients and predicted surface volumetric water content and temperature. The soil model was a two-layer force restore model adapted from Noilhan and Planton (1989). Finally, the simulations utilized the NASA Goddard Radiative Transfer Parameterization (Chou 1990,1992; Tao et al. 1996; Chou et al. 1998), in conjunction with the TIPA described earlier (Varnai and Davis 1999). In the TIPA, radiation can propagate slantwise when the solar zenith angle is less than 60 degrees. Each simulation employing the TIPA with shading was compared with a transparent cloud simulation (also using TIPA). The transparent cloud simulation served as the control simulation, in which cloud water, rain water, cloud ice, snow, and hail/graupel are all set to zero in calculating the incoming solar radiation. It was necessary for the control simulations also to include radiation so that the boundary layer would evolve like the sunny regions of the TIPA shading runs; otherwise, the TIPA shading and transparent simulation environments would be characterized by different CAPE and CIN, and quite likely different vertical shear as well, making it impossible to separate the influences of the cloud shading from differences in the storm environments.

3. Methodology

The TIPA shading runs were compared against transparent cloud runs in two different shear regimes. In one set of simulations, the zonal wind speed increased linearly from -10 m/s at the surface to 10 m/s at 2500 m above the surface. The initial zonal wind component was constant at 10 m/s above 2500 m. For the second set of simulations, the low level shear was specified as in the previous simulation; however, a second layer of wind shear was added above 7500 m, with the zonal wind increasing from 10 m/s at 7500 m to 30 m/s at 10,000 m. This second round of simulations was designed specifically to lengthen the anvil without changing the low level environment. Hereafter, these simulations will be referred to as the ”short anvil” and ”long anvil” simulations respectively.

Initial simulations were compared to the Bryan and Parker (2010) observations of a squall line passing over Cherokee, Oklahoma. Nine soundings were released in Cherokee, Oklahoma within 3 hours of a squall line passing over the town (the beginning stages of this squall line can be seen in Fig. 2).

Fig. 3 shows two of the soundings, one of which was released was released at 2138 UTC (in clear air), the other released after 90 minutes of anvil shading at 2307 UTC. When comparing the potential temperatures of the soundings to the model output (Fig. 4), one should note that the model noticeably mixes out much of the boundary layer, whereas the observed soundings under random fluctuations with greater amounts of surface cooling. The differences between the model profiles and observed profiles might suggest a deficiency in the models handling of vertical mixing (perhaps due to an inappro-

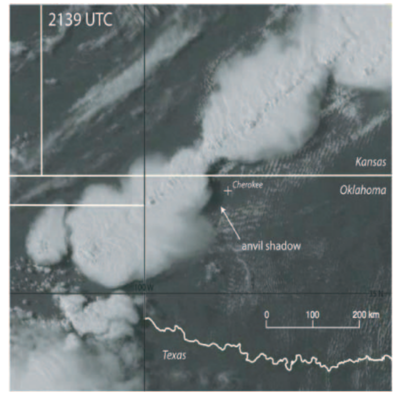

FIG. 2. Satellite image of the developing squall line at 2139 UTC (during the first clear air sounding release) from Bryan and Parker (2010).

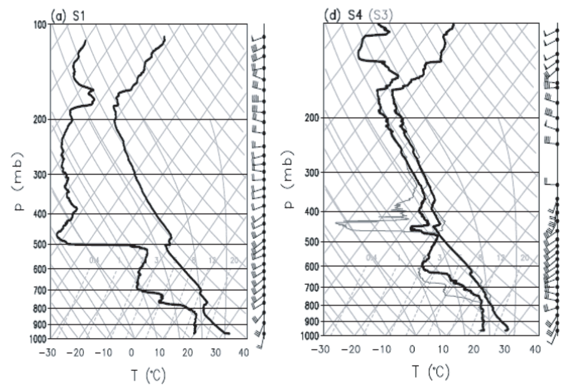

FIG. 3. Two soundings released by Bryan and Parker (2010). The left sounding was released at 2138 UTC in the clear air. The right sounding was released at 2307 UTC after ∼90 minutes of anvil shading.

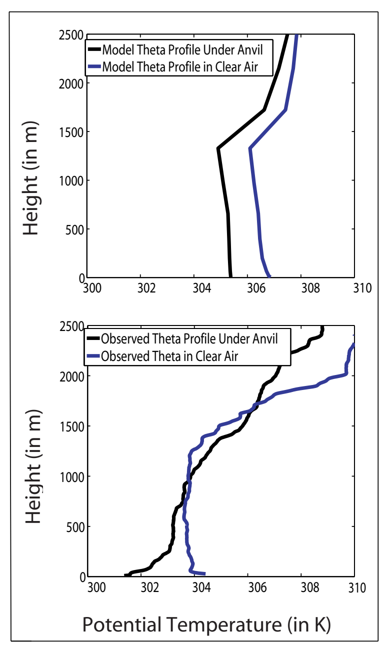

FIG. 4. Bryan and Parker’s (2010) observations of potential temperature profiles in lowest 2500 m under the anvil compared to the shading simulation model output of potential temperature under the anvil.

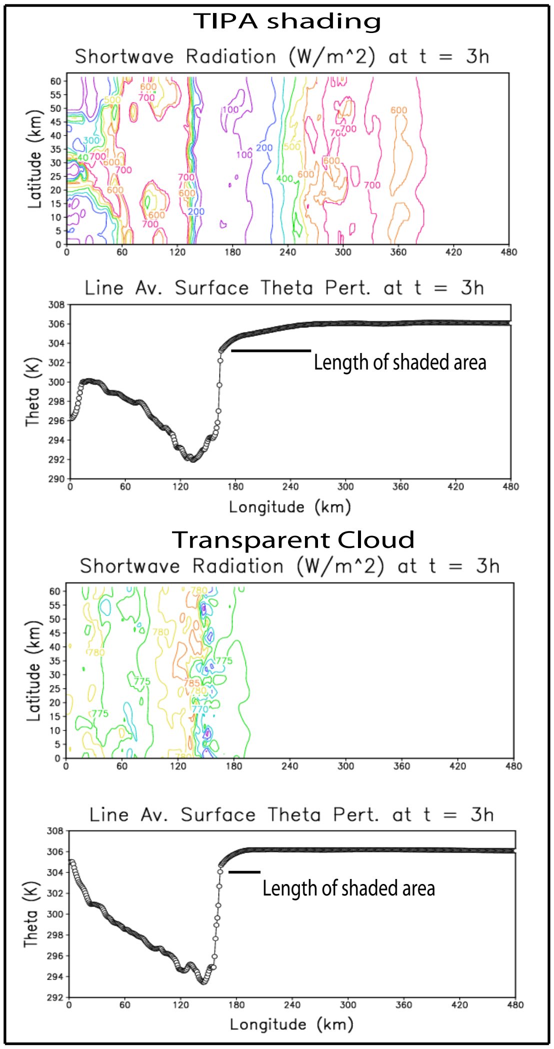

FIG. 5. Differences in radiation values and line averaged surface potential temperatures between the TIPA shading simulation and transparent cloud control simulation.

priate mixing length being used) or parameterization of surface fluxes. It is certainly within the realm of possibility that the forthcoming results might underestimate the dynamical influence of cloud shading given the large discrepancies between the observed and simulated static stabilities ahead of the squall lines (the simulations greatly underdo the increase in static stability within the anvil shadow), which might imply significant differences in the evolution of the vertical wind profiles in the near-storm environments (and ultimately the characteristics of the gust front updraft and overlying squall line structure).

4. Results

Throughout the course of the simulations, differences in squall line propagation and structure were observed. In fact, differences in the shortwave radiation field and the effects on the line averaged potential temperature profile between the transparent and TIPA shading simulations become apparent after just 3 hours (Fig. 5). As the simulations continued to evolve, noticeable differences became apparent also in the horizontal and vertical velocity fields. Figure 6 shows the differences in the short anvil runs after 5 hours into the simulations. The potential temperature field illustrates noticeable differences in cold pool strength, and these differences are manifested by the position of the gust front at the end of the simulation. The edge of the gust front in the stronger cold pool (i.e. shading case), has propagated past 250 km in the domain by 5 hours. The leading edge of the weaker cold pool in the transparent case had not yet reached 230 km by 5 hours. The stronger cold pool in the shading case can be explained by the greater vertical velocities (and therefore more trailing precipitation).

An examination of the longer anvil cases reveals a surprising reversal in squall line strength. Figure 7 shows the differences in the longer anvil case. In this case, the transparent run has a noticeably stronger cold pool, owing most likely to greater vertical velocities. Also, the position of the leading edge of the transparent case gust front appears to be approximately 30 km ahead of the shading case after 5 hours. The difference between the short anvil and long anvil cases raises an important set of fundamental questions concerning the evolution of the wind profile in different shading scenarios.

Upon inspection of the wind profiles, each of the profiles displayed a reversal in the 2.5 km shear ahead of the gust front. According to Rotunno et al. (1988), the 0 – 2.5 km shear, along with the cold pool strength, are the determining factors for squall line strength and longevity. In fact, the wind profiles, and thus the 0–2.5 km shear, do evolve quite differently in each simulation (Fig. 8). In all of the simulations, there is a shallow layer of easterly shear (to $\sim$700m) in the surface layer. This is to be expected as a result of surface drag. All of the profiles have an easterly wind maximum between 500 – 800 m above which the shear regime becomes westerly again. Each of the profiles have a similar shape, so the magnitude of surface layer easterly shear and surface friction actually have a profound impact on how much 0 – 2.5 km westerly shear each profile will have. Thus, even though the wind profiles have evolved in a similar way, the slight differences in surface layer shear actually exert a net impact on which profiles will have more deep layer westerly shear. Fig. 9 shows a plot of the Rotunno et al. (1988) parameter '$c/\Delta u$'. The short anvil TIPA shading and long anvil transparent cases are less suboptimal (from the Rotunno et al. (1988) standpoint of optimal balance) than their counterparts.

5. Questions for ongoing research

The results of these simulations suggest several different avenues for future exploration. It has been shown that the longer anvil does not enhance the differences in squall line propagation, as one might think, but rather reverses the difference, so that the transparent cloud model run shows a stronger and more intense squall line. The differences in the outcomes of the simulations are well predicted by differences in how the low–level wind shear within the shading region evolves ahead of the gust fronts. The simulations experiencing the largest reductions in pre–gust front westerly shear (for a given cold pool strength) produce the weakest squall lines, as

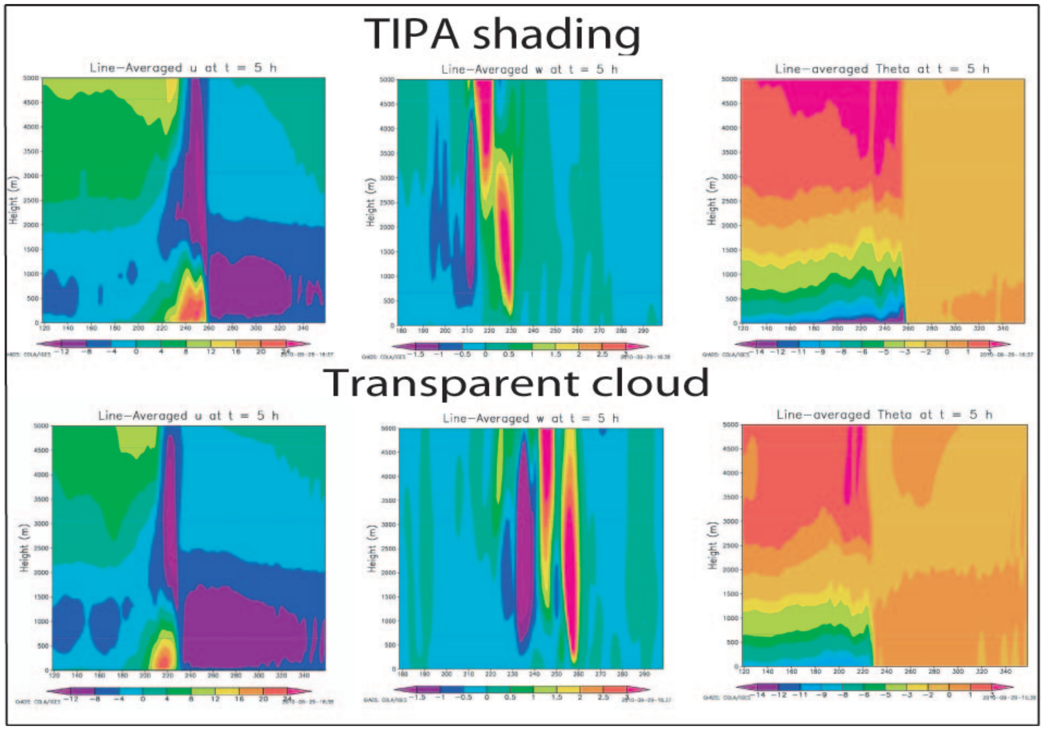

FIG. 6. Differences in vertical velocity, zonal velocity, and potential temperature after 5 hours in the short anvil simulations.

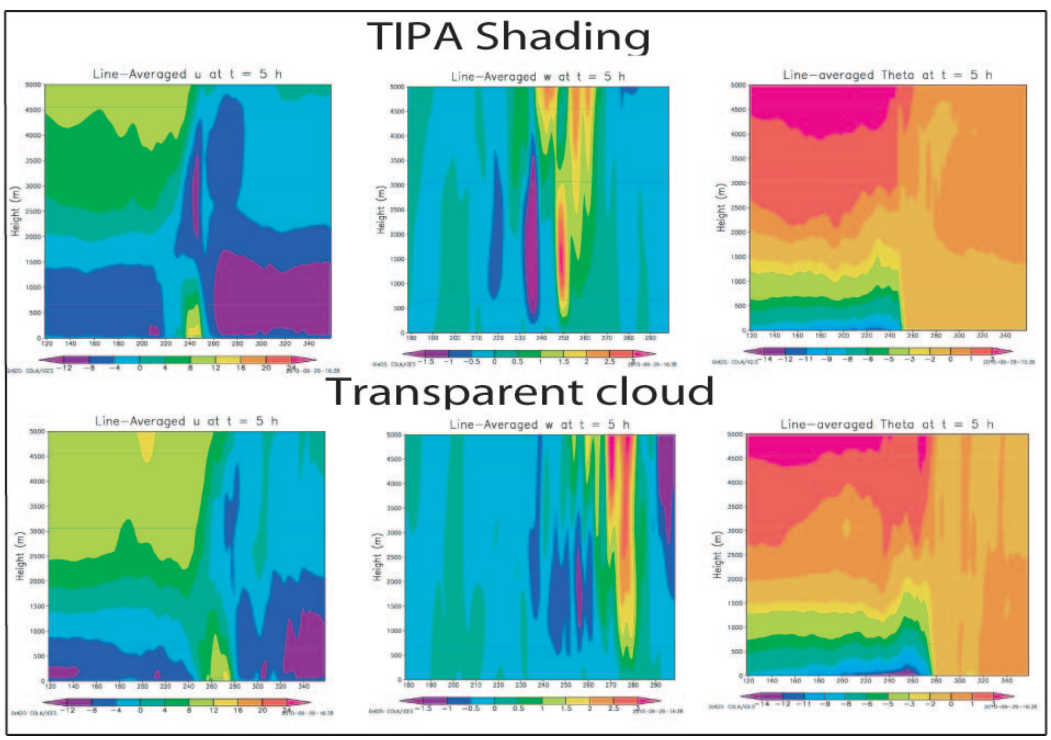

FIG. 7. Differences in vertical velocity, zonal velocity, and potential temperature after 5 hours in the long anvil simulations.

would be expected from Rotunno et al.'s (1988) definition of the optimal state. Logically, our next pursuit is an investigation of the dynamics underlying the changes in the pre–gust front wind profiles. Our near–term efforts will examine the vorticity budget of the inflow in order to assess the influence of baroclinic vorticity generation versus the reduction of vertical mixing on the horizontal vorticity within the shaded inflow region.

Acknowledgments. We wish to thank Jeff Frame for his insight and help in preparing the model. Also, we would like to acknowledge support from NSF grant ATM-0644533 which helped fund this research.

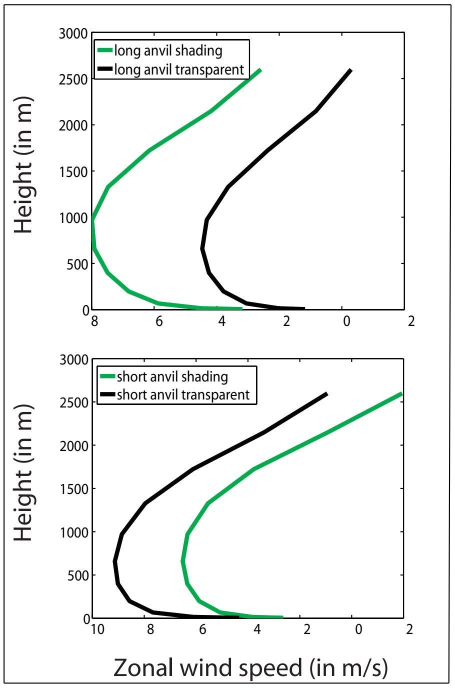

FIG. 8. Difference in the area–averaged zonal wind profiles (averaged 5–15 km ahead of the gust front) between the TIPA shading simulations and the transparent cloud control simulations at t = 4 hours.

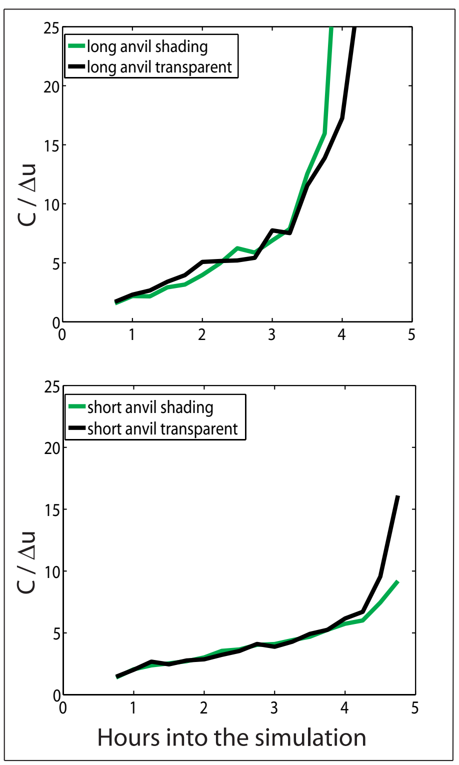

FIG. 9. Differences in the average parameter '$c/\Delta u$' (as referenced in Rotunno et al. 1988)) over the simulation time. In this formulation, 'c' is the area-averaged cold pool strength (averaged 0–10 km behind the gust front), and Δu is the zonal wind shear (averaged 5–15 km ahead of the gust front).

REFERENCES

Bryan, G.H., and M.D. Parker, 2010: Observations of a squall line and its near environment using high-frequency rawinsonde launches during VORTEX2. *Mon. Wea. Rev.*, accepted in final form May 2010.

Cahalan, R. F., L. Oreopoulos, A. Marshak, K. F. Evans, A. Davis, R. Pincus, K. Yetzer, B. Mayer, R. Davies, T. Ackerman, H. Barker, E. Clothiaux, R. Ellingson, M. Garay, E. Kassianov, S. Kinne, A. Macke, W. OHirok, P. Partain, S. Prigarin, A. Rublev, G. Stephens, F. Szczap, E. Takara, T. Varnai, G. Wen, and T. Zhuravleva, 2005: The International Intercomparison of 3D Radiation Codes (I3RC): Bringing together the most advanced radiative transfer tools for cloudy atmospheres. *Bull. Amer. Meteor. Soc.*, **86(9)**, 1275–1293.

Chou, M.-D., 1990: Parameterization for the absorption of solar radiation by O2 and CO2 with application to climate studies. *J. Climate*, **3**, 209–217

Chou, M.-D., 1992: A solar radiation model for climate studies. *J. Atmos. Sci.*, **49**, 762–772.

Chou, M.-D., M.J. Suarez, C.-H. Ho, M. M.-H. Yan, and K.-T. Lee, 1998: Parameterizations for cloud overlapping and shortwave single-scattering properties for use in general circulations and cloud ensemble models. *J. Climate*, **11**, 202–214.

Frame, J., P.M. Markowski, and J. Petters, 2008: The dynamical influences of cloud shading on simulated supercell environments. *The 24th Conference on Severe Local Storms*, Savannah, GA, American Meteorology Society, 17.B1

Frame, J. and P. Markowski, 2008: Simulations of a supercell thunderstorm with radiative transfer, surface physics, and a soil model. *The 24th Conference on Severe Local Storms*, Savannah, GA, American Meteorological Society, 16.6.

Frame, J., J. L. Petters, P. Markowski, and J. Harrington, 2009: An application of the tilted independent pixel approximation to cumulonimbus environments. *Atmospheric Research*, **91**, 127–136.

Frame, J. and P. Markowski, 2010: Numerical simulations of radiative cooling beneath the anvils of supercell thunderstorms. *Mom. Wea. Rev.*, **138:8**, 3024–3047.

Lin, Yuh-Lang, Richard D. Farley, Harold D. Orville, 1983: Bulk parameterization of the snow field in a cloud model. *J. Climate Appl. Meteor.*, **22**, 1065–1092.

Marchuk, G., G. Mikhailov, M. Nazaraliev, R. Darbinjan, B. Kargin, and B. Elepov, 1980: it The Monte Carlo methods in atmospheric optics. Springer-Verlag, 208pp.

Markowski, P. M., E. N. Rasmussen, J. M. Straka, and D.C. Dowell, 1998: Observations of low-level baroclinity generated by anvil shadows. *Mon. Wea. Rev.*, **126**, 2942–2958.

Markowski, P. M. and J. Harrington, 2005: A simulation of a supercell thunderstorm with emulated radiative cooling beneath the anvil. *J. Atmos. Sci.*, **62**, 2607–2617.

Marshak, A., W. J. Wiscombe, and R. F. Cahalan, 1995: Radiative smoothing in fractal clouds. *J. Geophys. Res.*, **100(26)**, 26247-26261.

Noilhan, J. and S. Planton, 1989: A simple parameterization of land surface processes for meteorological models. *Mon. Wea. Rev.*, **117**, 536–549

O'Hirok, W. and C. Gautier, 2005: The impact of model resolution on differences between independent column approximation and Monte Carlo estimates of shortwave surface irradiance and atmospheric heating rate. *J. Atmos. Sci.*, **62**, 2939–2951.

Rotunno, R., J. B. Klemp, M. L. Weisman, 1988: A theory for strong, long-lived squall lines. *J. Atmos. Sci.*, **45**, 463–485.

Sun, W.-Y. and C.-Z. Chang, 1986: Diffusion model for a convective layer. Part I: Numerical simulation of convective boundary layer. *J. Climate Appl. Meteor.*, **126**, 2942–2958.

Markowski, P. M. and J. Harrington, 2005: A simulation of a supercell thunderstorm with emulated radiative cooling beneath the anvil. *J. Atmos. Sci.*, **25**, 1445–1453.

Tao, W.-K., S. Lang, J. Simpson, C.-H. Sui, B. Ferrier, and M.-D. Chou, 1996: Mechanisms of cloud-radiation interaction in the tropics and mid-latitude. *J. Atmos. Sci.*, **53**, 2624-2651.

Vrnai, T. and R. Davies, 1999: Effects of cloud heterogeneities on shortwave radiation: comparison of cloud-top variability and internal heterogeneity. *J. Atmos. Sci.*, **56**, 4206–4224.

Xue, M., Droegemeier, K.K., Wong, V., 2000: The Advanced Regional Prediction System (ARPS): a multiscale nonhydrostatic atmospheric simulation and prediction tool. Part I: Model dynamics and verification. *Meteorol. Atmos. Phys.*, **75**, 161–193.

Xue, M., K.K. Droegemeier, V. Wong, A. Shapiro, K. Brewster, F. Carr, D. Weber, Y. Liu and D.H. Wang, 2001: The Advanced Regional Prediction System (ARPS): a multiscale nonhydrostatic atmospheric simulation and prediction tool. Part II: Model physics and applications. *Meteorol. Atmos. Phys.*, **76**, 143–165.